The Intensity-dependence of Tropical Cyclone Intensification Rate in a Simplified Energetically Based Dynamical System Model

Yuqing Wang[1*], Yuanlong Li[2,1], Jing Xu[3], Zhe-Min Tan[4], and Yanluan Lin[2]

[1]International Pacific Research Center and Department of Atmospheric Sciences, University of Hawaii at Mānoa, Honolulu, HI 96822

[2]Ministry of Education Key Laboratory for Earth System Modeling, Department of Earth System Science, and Joint Center for Global Change Studies (JCGCS), Tsinghua University, Beijing, China.

[3]State Key Laboratory of Severe Weather, Chinese Academy of Meteorological Sciences, China Meteorological Administration, Beijing, China

[4]Key Laboratory of Mesoscale Severe Weather/MOE, and School of the Atmospheric Sciences, Nanjing University, Nanjing, China

December 21, 2020 (submitted)
March 5, 2021 (first revision)
April 7, 2021 (second revision)
Dateline

Submitted to ***Journal of the Atmospheric Sciences***

Corresponding author: Prof. Yuqing Wang
Room 404A, IPRC/SOEST
University of Hawaii at Manoa
1680 East-West Road
Honolulu, HI 96822
Email: yuqing@hawaii.edu

Abstract

In this study, a simple energetically based dynamical system model of tropical cyclone (TC) intensification is modified to account for the observed dependence of the intensification rate (IR) on the storm intensity. According to the modified dynamical system model, the TC IR is controlled by the intensification potential (IP) and the weakening rate due to surface friction beneath the eyewall. The IP is determined primarily by the rate of change in the potential energy available for a TC to develop, which is a function of the thermodynamic conditions of the atmosphere and the underlying ocean, and the dynamical efficiency of the TC system. The latter depends strongly on the degree of convective organization within the eyewall and the inner-core inertial stability of the storm. At a relatively low TC intensity, the IP of the intensifying storm is larger than the frictional weakening rate, leading to an increase in the TC IR with TC intensity in this stage. As the storm reaches an intermediate intensity of 30-40 m s^{-1}, the difference between IP and frictional weakening rate reaches its maximum, concurrent with the maximum IR. Later on, the IR decreases as the TC intensifies further because the frictional dissipation increases with TC intensity at a faster rate than the IP. Finally, the storm approaches its maximum potential intensity (MPI) and the IR becomes zero. The modified dynamical system model is validated with results from idealized simulations with an axisymmetric nonhydrostatic, cloud-resolving model.

1. Introduction

Upon the genesis of a tropical depression under favorable environmental conditions, such as high sea surface temperature (SST) and high heat content in the uppermost ocean layer, and weak vertical wind shear (Gray 1979), the cyclonic low-pressure system may develop into a tropical cyclone (TC) of tropical storm strength with a maximum sustained surface wind speed higher than 17 m s^{-1}. In the absence of deleterious environmental effects, a TC often experiences a phase of rapid intensification (RI) associated with an increase in near-surface maximum wind speed of more than 15 m s^{-1} per day, before it reaches its maximum intensity (Wang and Wu 2004). Over the past five decades or so, many efforts have been devoted to conceptualizing the physical mechanisms that are responsible for TC intensification. Montgomery and Smith (2014) summarized and compared four most prominent paradigms of TC intensification in the literature. These are the CISK paradigm (conditional instability of the second kind, Charney and Eliassen 1964); the cooperative intensification paradigm (Ooyama 1964, 1969, 1982); the thermodynamic air-sea interaction intensification paradigm (namely, the wind-induced heat exchange feedback – WISHE, Rotunno and Emanuel 1987; Emanuel 1988, 1989, 1995, 1997; Emanuel et al. 1994); and the rotating convective paradigm (Nguyen et al. 2008; Montgomery et al. 2009; Smith et al. 2009). Each of these paradigms give, to some extent, a qualitative explanation for the intensification processes[1], but none of these concepts provides a quantitative

[1]Note that we are not going to discuss the advantages and disadvantages of each paradigm here. Readers are referred to a review paper by Montgomery and Smith (2014) for details. Nevertheless, we will provide new insights into the question on what are the predominant processes leading to TC intensification.

measure of the intensification rate (IR) of a TC.

Unlike the maximum potential intensity (MPI), i.e., the maximum intensity a TC may reach during its lifetime under given favorable environmental conditions, the TC IR cannot be treated under the assumption of a system in balanced steady state. Moreover, the IR of a TC may be affected by many more factors than MPI, such as instantaneous storm intensity, the radial location of diabatic heating, and both the inner and outer core structures of the TC, etc. (Schubert and Hack, 1982; Vigh and Schubert 2009; Pendergrass and Willoughby 2009; Rogers et al. 2013; Carrasco et al. 2014; Xu and Wang 2015, 2018a,b). Recent studies based on best track TC data have provided evidence of some robust relationships between the TC IR and the inner and outer core sizes (Carrasco et al. 2014; Xu and Wang 2015, 2018a) and the TC intensity (Kaplan et al. 2010; Xu and Wang 2015, 2018a). Figure 1, which is adopted from Xu and Wang (2018a, see their Fig. 6), shows the frequency of subsequent 24-h IR against TC intensity, together with the 95th percentile of IR in different SST bins over the western North Pacific (WNP) during 1982-2015 based on the best track data from the Joint Typhoon Warning Center (JTWC). Overall, it can be seen that the IR increases with TC intensity if the 10-m sustained maximum wind speed (V_{max}) is below about 60-70 knots (or 30-36 m s^{-1}), an intensity range corresponding to TCs of about category-1 hurricane strength as defined by the Saffir-Simpson wind scale. In addition, it is obvious that the overall IR increases with SST, consistent with recent axisymmetric numerical simulations (Li et al. 2020).

The observed initial increase in the TC IR with TC intensity is often explained by the balance dynamics extensively studied by Shapiro and Willoughby (1982), Schubert and Hack

(1982) and Pendergrass and Willoughby (2009). These studies showed that storms at greater intensity tend to have a higher inner-core inertial stability and thus higher heating efficiency to intensify the TC. However, the IR in observations tends to decrease with TC intensity once the storm becomes stronger than 60-70 knots (cf. Fig. 1). To explain this, it has been suggested that in an intensifying TC getting close to its MPI, the enhanced heating efficiency is mostly offset by the surface frictional dissipation effect (Kaplan et al. 2010; Xu and Wang 2015). Kaplan et al. (2010) also hypothesized that TCs of a certain intensity, which are sufficiently well organized but relatively far from their MPI, are likely to undergo RI.

Although several previous studies have derived time-dependent equations for TC intensity change (namely, IR) under various assumptions based on concepts of different complexities (DeMaria 2009; Emanuel 1997, 2012; Ozawa and Shimokawa 2015; Emanuel and Zhang 2017), the intensity-dependent IR with the maximum at an intermediate intensity as shown in observations has not been well discussed yet. In this study, we augment the energetically based dynamical system model conceptualized by Ozawa and Shimokawa (2015) to account for the intensity-dependence of the TC IR as evident from best-track TC data analyses as presented in Kaplan et al. (2010) and Xu and Wang (2015, 2018a). Modifications to the simple energetically based dynamical system model of a TC based on the viewpoint of a non-steady-state Carnot heat engine is introduced in section 2. The modified model may serve to physically explain and quantify the observed intensity-dependence of the TC IR. Some assumptions made in the derivation of the simplified model are evaluated in section 3 based on results from idealized axisymmetric numerical simulations. Major conclusions are drawn in the last section.

2. A modified energetically based dynamical system model for TC intensification

In this section, we discuss a modification to an energetically based conceptual model, which allows us to capture and quantify the intensity dependence of the TC IR as obtained from the best track TC data over the WNP (Fig. 1). As in earlier studies, we start with the basic concept on energy production and frictional dissipation processes in a TC system, where the TC is energetically considered as a Carnot heat engine after it has developed a well-defined eyewall structure (cf. Kleinschmidt, 1951; Emanuel, 1988, 1997; Wang and Xu, 2010, Schönemann and Frisius 2012). For a detailed elaboration of the thermodynamic fundamentals underlying this concept, we refer the readers to the paper by Ozawa and Shimokawa (2015). Our working hypothesis is that the TC intensifies, as measured by the increase in mechanical energy in the inner core, when there is a positive net energy gain rate due to the imbalance between the energy production and frictional dissipation rates. Here, we extend the commonly used framework to describe TC energetics by introducing a normalized inertial stability factor, which acts on the effective power generation, thereby modifying the intensification potential (IP) of the TC. The inertial stability factor is introduced to account for the dynamical efficiency of eyewall heating, thus making the conceptual model applicable to weak TC systems as will be detailed below.

From a heat engine perspective, almost all energy input to a TC system comes from the ocean beneath. Hence, the mechanical energy production rate or power generation (P_E) chiefly depends on the enthalpy flux from the underlying ocean and the thermodynamic efficiency of the heat engine (TC system). For a well-organized TC system, P_E can be expressed as (Emanuel

1997)

$$P_E = \int \varepsilon C_k \rho \left|\vec{V}\right| (\kappa_o^* - \kappa_a) r dr d\lambda, \tag{1}$$

where r is radius, λ the azimuth, C_k the surface exchange coefficient for enthalpy (or "heat"), ρ the air density near the surface, $\left|\vec{V}\right|$ the near surface wind speed, κ_o^* the saturated enthalpy of the ocean surface at a given SST (T_S), κ_a the enthalpy of the atmosphere near the surface, and ε the thermodynamic efficiency[2] of the heat engine, which is determined by the difference between T_S and the outflow layer air temperature (T_O). On the other hand, the mechanical energy is dissipated to the underlying ocean due to surface friction. The frictional energy dissipation rate or power dissipation (F_D) can be written as (Emanuel 1997)

$$F_D = \int C_D \rho \left|\vec{V}\right|^3 r dr d\lambda, \tag{2}$$

where C_D is the surface drag coefficient.

Theoretically, the area integrations in Eqs. (1) and (2) should be taken over the whole TC system. However, both integrals are dominated by fluxes in the eyewall region near the radius of maximum wind (RMW, r_m). On this basis, and assuming the inner region to be quasi-axisymmetric, Emanuel (1997) argued that in a mature TC at maximum intensity the power generation and frictional dissipation as given by Eqs. (1) and (2) are balanced [cf. Eq. (7) in Emanuel 1997]

---

[2] Note, when the effect of dissipative heating is neglected, the thermodynamic efficiency is given by $\varepsilon = \frac{T_S - T_O}{T_S}$. When the dissipative heating effect is included, the denominator is changed from T_S to T_O: $\varepsilon = \frac{T_S - T_O}{T_O}$ (Bister and Emanuel 1998). Under mean tropical conditions, the consideration of dissipative heating is equivalent to an increase in ε from about 1/3 to 1/2, which can result in a 22.5% increase in MPI. Both T_S and T_O are considered as unperturbed environmental parameters in the original MPI theory of Emanuel (1988).

$$\int_{r_m}^{r_o} \rho \epsilon C_k \left|\vec{V}\right| (\kappa_o^* - \kappa_a) r dr = \int_{r_m}^{r_o} \rho C_D \left|\vec{V}\right|^3 r dr, \tag{3}$$

and that the integrands of Eq. (3) can be equated to a good approximation at r_m to get

$$\rho \epsilon C_k \left|\overrightarrow{V_{mpi}}\right| (\kappa_o^* - \kappa_a)|_{r_m} = \rho C_D \left|\overrightarrow{V_{mpi}}\right|^3 |_{r_m}. \tag{4}$$

Rearranging Eq. (4) gives the MPI in terms of the maximum near surface wind speed:

$$V_{mpi} = \sqrt{\frac{C_k}{C_D} \varepsilon (\kappa_o^* - \kappa_a)|_{r_m}}. \tag{5}$$

Since we aim to understand the intensification process of a TC, we focus on the transient (non-equilibrium) stage after the initial cyclogenesis phase and before the TC gets close to its MPI. If all diabatic heating released in eyewall convection were most efficiently deployed to warm the TC core, and hence to intensify the TC system, the time-dependent energy gain rate (EGR per unit area) equation for an axisymmetric TC system could be simply expressed in terms of the difference between power generation P_E and power dissipation F_D:

$$EGR = P_E - F_D = \rho \epsilon C_k \left|\vec{V}\right| (\kappa_o^* - \kappa_a)|_{r_m} - \rho C_D \left|\vec{V}\right|^3 |_{r_m}. \tag{6}$$

However, as elaborated in Schubert and Hack (1982, see their section 3, 1983, see their Fig. 7), the heating efficiency, i.e., the degree to which convective heating is used to warm the inner core, chiefly depends on the inertial stability within the RMW. Shapiro and Willoughby (1982) and Pendergrass and Willoughby (2009) also demonstrated that the efficiency increases with increasing storm intensity. Based on these studies, we argue that the effective power generation for the TC system, which represents the actual intensification potential (IP) of a TC, can be well approximated by the product of P_E and a dynamical efficiency factor E, rather than P_E alone. To the first option, we assume that the dynamical efficiency E is a function of the inertial stability frequency, I, in the TC core normalized by the inertial stability frequency of the mature storm at its MPI, I_{mpi}:

$$E = \left(\frac{I}{I_{mpi}}\right)^n = [\frac{\sqrt{\left(f+\frac{2V}{r}\right)\left(f+\frac{\partial rV}{r\partial r}\right)}|_{r_m}}{\sqrt{\left(f+\frac{2V}{r}\right)\left(f+\frac{\partial rV}{r\partial r}\right)}|_{rmpi}^{mpi}}]^n, \tag{7}$$

where the power constant n is introduced as a measure of TC IR sensitivity to the functional relationship with the normalized inertial stability frequency. To incorporate the dynamical efficiency dependence of the IP, we modify Eq. (6) formulating the EGR per unit area as follows:

$$EGR = EP_E - F_D = E\rho\epsilon C_k\left|\vec{V}\right|(\kappa_o^* - \kappa_a)|_{r_m} - \rho C_D\left|\vec{V}\right|^3|_{r_m}. \tag{8}$$

The dynamical efficiency factor E is introduced to consider the cases in which the inner-core inertial stability is small, or the corresponding local Rossby radius of deformation is large, most of latent heating in the eyewall is diverted to energy of gravity waves propagating away from the inner core region of a TC system and thus contributing little to TC intensification. As the TC intensifies and the inner-core inertial stability increases, more energy will be partitioned to fuel the rotational component of the local circulation in the inner core along with an increase in the local mechanical energy, and thus the IP of the TC system with some energy being consumed to spin up the upper-tropospheric anticyclonic circulation as the eyewall forms (Emanuel 2012). If we simply assume a solid body rotation in the eye region and estimate the inner core inertial stability inside the RMW, Eq. (7) can be approximated by

$$E_{sim} = (\frac{f+\frac{2V_m}{r_m}}{f+\frac{2V_{mpi}}{r_{mpi}}})^n, \tag{9}$$

where V_m is the time-dependent near-surface maximum tangential wind of the TC vortex, V_{mpi} is the corresponding MPI, r_m is the RMW of the intensifying TC, and r_{mpi} is the RMW of the storm at its MPI. Equation (7) or (9) implies that the dynamical efficiency of the TC system becomes

100% when the storm reaches its MPI, while it is quite low in the incipient stage of the system.

By definition, a non-zero EGR [Eq. (8)] will lead to a change in the mechanical energy in the inner core near the RMW in the eyewall region, i.e.,

$$EGR = \rho H \frac{d}{dt}\left(\frac{1}{2}\left|\vec{V}\right|^2\right)|_{r_m}, \tag{10}$$

where H is the height parameter, and has been considered as the density scale height of the atmosphere in Ozawa and Shimokawa (2015) because they focus on the whole TC system and the average wind speed of the whole TC system. However, we focus on the inner-core region and the near surface maximum wind speed. Therefore, the H can be understood as the height of air column per unit area near the RMW with the average wind speed in this column being $\left|\vec{V}\right||_{r_m}$, and is in an amount that the average mechanical energy in this "virtual" column is determined by the local EGR [Eq. (8)]. The definition of H in practice will be discussed in detail later.

Considering the fact that the changes of $\epsilon C_k(\kappa_o^* - \kappa_a)$ and C_D with time are usually small compared to the change of maximum near surface wind speed (Li et al. 2020) and thus using the MPI-definition Eq. (5) and Eq. (10), Eq. (8) can be rewritten as[3]

$$\rho H \frac{d}{dt}\left(\frac{1}{2}V_{max}^2\right) = \rho C_D V_{max}[EV_{mpi}^2 - V_{max}^2], \tag{11}$$

or

$$\frac{\partial V_{max}}{\partial t} = \frac{C_D}{H}(EV_{mpi}^2 - V_{max}^2), \tag{12}$$

According to the modified energetically based intensification model given above, the IR of a TC is controlled by three major factors: 1) the potential energy available for the TC to intensify, i.e.,

[3]Note, for reasons of clarity, we will omit the subscript "r_m" for values near the RMW and write $\left|\vec{V}\right|_{r_m}$ as V_{max} hereafter.

the MPI determined by the thermodynamics of the atmosphere and the underlying ocean; 2) the dynamical efficiency of the eyewall heating, which depends strongly on the degree of convective organization in the eyewall and the inner-core inertial stability; and 3) the weakening rate due to surface friction. As outlined above, the first term on the rhs of Eq. (12) can be considered as the TC's IP, which is a function of the potential energy available for the TC to intensify and the dynamical efficiency of the eyewall heating, while the second term represents the weakening rate due to surface frictional dissipation. The dynamical efficiency that we have introduced is a function of the power index n and the inner-core inertial stability frequency. Note that if n is taken to be zero so that E equals one, Eq. (12) will become similar to Eq. (17) in Emanuel (2012). In addition, Eq. (12) is similar to Eq. (2) in Emanuel and Zhang (2017), however, the physical meanings are different. Here we mainly focus on the intrinsic inner-core dynamics but Emanuel and Zhang (2017) focused on parametrizing inner-core relative humidity and some other environmental conditions.

Figure 2 gives three examples of the IP (given by $\frac{C_D}{H}EV_{mpi}^2$) with different power constants (n = 0.0, 0.5 and 1.0) in the parameterized dynamical efficiency, the frictional weakening rate (FR, given by $\frac{C_D}{H}V_{max}^2$), and the resulting IR as a function of the instantaneous storm intensity (V_{max}) for V_{mpi} = 60 m s^{-1} at a radius of r_{mpi} = 15 km. The MPI value chosen here is roughly corresponding to conditions with an SST of 29°C over the tropical WNP, and E is calculated according to Eq. (9). Other parameters used in the calculations are $C_D = 2.4\times10^{-3}$, $C_k = 1.2\times10^{-3}$, $f = 5\times10^{-5}$, and H = 3 km (as in Emanuel and Zhang 2017). Note that, for simplicity, we have not considered the contraction of r_m during the intensification stage of the TC and assumed r_m is the same as r_{mpi} in the examples shown. Considering r_m is usually larger than r_{mpi} for weak systems (Li et al. 2019), the IR on the weak V_{max} side would become smaller for $n > 0$. In case n =0 (black curves in Fig. 2), which is equivalent to $E = 1$ (as in Emanuel 2012), the potential energy available can be fully used to intensify the TC and thus the IP for $E = 1$ (dotted black curve) is independent of the instantaneous TC intensity. Since in all cases, the frictional weakening rate FR (solid blue curve) increases with the square of V_{max}, the IR for $E = 1$ (dashed black curve) would be maximal when $V_{max} = 0$ and decreasing monotonously as the TC intensifies. In that case, a maximum IR of ~250 m s^{-1} d^{-1} is obtained, which has never been reported from nature. Although the maximum IR may be reduced with larger H, it still occurs at $V_{max} = 0$, which is not consistent with the finite-amplitude nature of TC genesis/development described in Emanuel (1989). Furthermore, the monotonous decrease in IR with increasing TC intensity is in contrast to the observed intensity-dependence of the TC IR which exhibits a maximum at intermediate intensity (cf. Fig. 1).

For both $n = 0.5$ (red curves) and 1.0 (green curves), the IP at low TC intensity is considerably reduced because of the low dynamical efficiency due to weak inner-core inertial stability. In both cases, the IR exhibits a maximum at an intermediate intensity. For $n = 0.5$, the maximum IR reaches about 120 m s^{-1} d^{-1} at a maximum near surface wind speed of about 25 m s^{-1}, while for $n = 1.0$, the maximum IR reaches 60 m s^{-1} d^{-1} at $V_{max} = 30$ m s^{-1}. Thus, the modified conceptual model given by Eq. (12) provides a reasonable upper limit to the maximum IR with $n = 1.0$ and it captures the overall intensity-dependence of the TC IR as found in observations (cf. Fig. 1). This strongly suggests that the introduction of the dynamical efficiency to the simplified energetically based dynamical system model of TC intensification is physically meaningful and thus acceptable to reproduce the intensity-dependence of TC IR in agreement with that from observational studies (Kaplan et al. 2010; Xu and Wang 2015, 2018a).

To find the TC intensity where the IR reaches its maximum, i.e., the maximum potential IR (MPIR), we differentiate Eq. (12) with respect to V_{max}. Assuming C_D and H are constant, the IR of the TC reaches a maximum when

$$\frac{\partial}{\partial \mathrm{V_{max}}}\left(\frac{dV_{max}}{dt}\right) = \frac{C_D}{H}\left(V_{mpi}^2 \frac{\partial E}{\partial V_{max}} - 2V_{max}\right) = 0,$$

namely,

$$V_{mpir} = \frac{V_{mpi}^2}{2} \frac{\partial E}{\partial V_{max}}, \tag{13}$$

Note, in deriving Eq. (13) from Eq. (12), the possible dependences of the thermodynamic efficiency, the surface exchange coefficients, and the enthalpy gradient across the air-sea interface on the surface wind speed near r_m (which are all implicitly included in the MPI) have been ignored. We argue that this is a reasonable approximation in the context of a conceptual dynamical system model since the effect is often quite small [cf. Fig. 1 in Emanuel (2012)]. Equation (12) indicates that the intensity-dependent nature of the TC IR depends strongly on the power index n related to the dynamical efficiency E of the TC system. Figure 3 shows the numerical solution of the dependence of the maximum wind speed V_{max} at which the IR reaches its maximum (V_{mpir}) on the power index n. As n increases, the MPIR decreases and occurs at relatively higher maximum wind speeds. Comparing Figs. 1 and 2, we can find that an n-value around 1.0 is reasonable for the chosen H and other parameters to a large extent. In the case shown, the MPIR can reach up to 60 m s^{-1} d^{-1} at a maximum wind speed around 30 m s^{-1}. Hence, the MPIR provides a reasonable upper limit to the maximum IR (Fig. 1), in a similar way to the MPI, which gives an upper limit to the maximum potential intensity, given favorable atmospheric and oceanic thermodynamic conditions.

Kaplan et al. (2010) hypothesized that the turning point from a positive to a negative correlation between the TC intensity and the corresponding IR (as shown in Fig. 1) may be associated with a balance between the thermodynamic/dynamic efficiency in response to eyewall heating and the potential of the TC to intensify towards its MPI. Our modified energetically based dynamical system model above quantifies this hypothesis and can reproduce the observed intensity-dependence of the TC IR reasonably well. Therefore, with the introduction of the dynamical efficiency as a factor in the IP of the TC system, the energetically based TC intensification model has potential to be used for real TC intensity forecasts as it captures the major features of the intensity-dependence of the TC IR as evident from observational data. Note that, from a forecast perspective, both the steady-state intensity (MPI) and RMW in the model should be estimated in advance. In addition, the dynamical efficiency discussed in this study can be considered the intrinsic dynamical efficiency of the TC vortex. In reality, many other factors may limit the dynamical efficiency, such as the environmental vertical wind shear and translation of the TC itself. However, as our first effort, we have only focused on the intrinsic dynamical efficient in this study.

3. Results from idealized full-physics model simulations

The modified energetically based dynamical system model for the TC IR outlined in section

2 is heavily conceptualized. To examine the extent to which the simplified model is valid, a series of ensemble numerical experiments are performed using the state-of-the-art axisymmetric Cloud Model 1 (CM1; Bryan and Fritsch 2002). Considering the TC IR varies with SST (Fig. 1), to ensure the robustness of the main results, experiments with different SST are performed. The experimental design follows the SST-dependent sounding experiments in Li et al. (2020) to ensure the consistency between SST and initial atmospheric sounding as in nature. There are four ensemble experiments with different SST and corresponding atmospheric sounding sorted for the WNP (labeled as SST28_WNP–SST31_WNP), and four ensemble experiments those sorted for the North Atlantic (NA; labeled as SST27_NA–SST30_NA). Each ensemble experiment has 21 runs. In the standard run the maximum tangential wind speed of the initial TC vortex is 15 m s^{-1} at the surface with the RMW of 80 km, and in the other 20 runs the maximum tangential wind speed and the RMW are perturbed by ±0.1 m s^{-1} (for 10 runs) and ±0.4 km (for 10 runs), respectively. All experiments are run on an *f*-plane of 20°N in a quiescent environment with the model domain of 3100 km×25 km in the radial and vertical directions, respectively. The radial grid spacing is 1 km within 100-km radius and is stretched to 12 km at the lateral boundary. The vertical grid spacing is stretched below 5.5 km with a total of 59 vertical levels used for the model atmosphere. The microphysics scheme of Thompson et al. (2008) is used for cloud microphysical processes and cumulus convection is not considered. Newtonian cooling, capped at 2 K day^{-1}, is used to mimic radiative cooling (Rotunno and Emanuel 1987), and dissipative heating is not considered. The Smagorinsky scheme (Bryan and Fritsch 2002) is used to mimic subgrid-scale turbulent mixing with the horizontal and asymptotic vertical mixing

lengths being fixed at 700 m and 70 m as in Li et al. (2020), respectively. The wind-dependent surface drag coefficient (C_D) of Donelan et al. (2004), which increases with wind speed at low wind speeds (<25 m s^{-1}) but keeps a constant (2.4×10^{-3}) at high wind speeds, is used for surface stress calculation, while a constant exchange coefficient (C_k) of 1.2×10^{-3} is used for surface enthalpy flux calculation. All simulations are integrated for 240 h with hourly model outputs, and we only used the intensity evolution from the ensemble mean for each experiment of simulations in our following analyses to avoid effects of convective processes and cloud-scale motions.

Figure 4 shows the time evolution of the maximum 10-m wind speed (V_{max}) and the corresponding RMW of each of the ensemble simulations and their corresponding ensemble mean for all experiments. All storms started to intensify after an initial adjustment period, and the adjustment period decreases with increasing SST (Figs. 4a,b). For each experiment, the maximum IR occurs when the maximum storm intensity is between ~30-40 m s^{-1} similar to that found in observations (Fig. 1). For both basins the maximum IR increases with increasing SST as in observations (Fig. 1). The RMW undergoes a continuous contraction after an initial adjustment period. This continuous contraction of the RMW coincides with the early and rapid intensification of the simulated storms. Afterwards, the RMW decreases very slowly and the contraction stops well before the end of intensification in each experiment. This behavior is consistent with recent findings from both observations and idealized numerical simulations by Stern et al. (2015) and Li et al. (2019), who also found that the contraction of the eyewall and the RMW does not necessarily coincide with the RI-period. Note that although some transient variability occurs in the IR among the ensemble simulations, the overall trends are quite similar. Therefore, since our major interest is in the overall intensification of the simulated TCs, we only focus on the ensemble mean results instead of displaying each of the 21 simulations for each experiment in the following discussion.

Based on the diagnostic results of Wang and Xu (2010) and Li et al. (2020), in the steady state of the simulated TCs, the local power generation and frictional dissipation may not be balanced under the eyewall hypothesized in the MPI theory. This yields superintensity (or subintensity) in the simulation defined as

$$SI = \frac{SV_{max} - V_{mpi}}{V_{mpi}}, \tag{14}$$

where SV_{max} denotes the steady-state intensity of the simulated TCs. Li et al. (2020) also found that the superintensity decreases with increasing SST because of the increase in either convective activity in the TC outer core region or the theoretical MPI or both. Correspondingly, the net EGR (Eq. 8) during the transient (non-equilibrium) stage can be modified to

$$P_E - F_D = (1 + SI)^2 E\rho\epsilon C_k \left|\vec{V}\right| (\kappa_o^* - \kappa_a)|_{r_m} - \rho C_D \left|\vec{V}\right|^3 |_{r_m}. \tag{15}$$

Therefore, the simplified intensification Eq. (12) can be rewritten as

$$\frac{\partial V_{max}}{\partial t} = \frac{C_D}{H}\left[E(1 + SI)^2 V_{mpi}^2 - V_{max}^2\right]. \tag{16}$$

This means that from a forecast perspective, we should diagnose not only V_{mpi} but also SI in advance to estimate the IR by Eq. (16). However, here, as a first step, our major interest is only to examine the framework of the conceptual model. For simplicity, we thus rewrite Eq. (16) by using Eq. (14) to give

$$\frac{\partial V_{max}}{\partial t} = \frac{C_D}{H}[E \cdot SV_{max}^2 - V_{max}^2]. \tag{17}$$

By this modification, all variables in the energetically based IR Eq. (17) can be directly calculated from the ensemble mean of our axisymmetric CM1 simulations, except for the power index n in the dynamical efficiency given in Eq. (7) or (9) and the height parameter H. Specifically, the IR at each time t_0 is calculated as the change rate of V_{max} between $t_0 - 3h$ and $t_0 + 3h$, and the "real-time" C_D, inertial stability, and V_{max} on the rhs of Eq. (17) are determined as their average value between $t_0 - 3h$ and $t_0 + 3h$ in each simulation. In addition, we have filtered out the small-scale perturbations less than 8 km in radial direction using a spatial average as in Li et al. (2019). For all experiments, we only focus on the period with the defined IR being continuously positive, and the steady-state intensity is determined as the 6-h averaged intensity around the end point of the period of interest. Note that the overall results below are not sensitive to the different time steps (i.e., 6h here) qualitatively, and the diagnostic results will be smoother with larger time step (not shown).

Based on Emanuel (2012) and Emanuel and Zhang (2017), the height parameter H was roughly twice the depth of the boundary layer. Considering the fact that the characteristic height scale of the TC inner-core boundary layer, no matter in dynamic or thermodynamic definition, is usually between ~500–2000 m (Zhang et al. 2011), the height parameter H can be chosen between ~1000–4000 m. Figure 5 shows the scatter diagram of the diagnosed dynamical efficiency from Eq. (17) under different H based on the ensemble-mean results of all experiment, with three different forms of dynamical efficiency shown, i.e., in terms of the normalized inertial stability (E) in Eq. (7), the normalized simplified inertial stability (E_{sim}) in Eq. (9), and the normalized absolute vertical vorticity (E^2/E_{sim}). For each H, the distributions among the three different forms of dynamical efficiency are similar, especially between E and E_{sim} (first and second columns in Fig. 5), implying that the normalized simplified inertial stability Eq. (9) is a good approximation of the normalized inertial stability Eq. (7) to parameterize the dynamical efficiency. From Fig. 5, for H = 2000 m, we can find that for all the three forms of dynamical efficiency, all the diagnostic results are smoothly distributed around the line of $n = 1$. However, with the varying H, more nonconstant power indices (n) are needed to capture the overall diagnostic results. Therefore, the settings $H = 2000\,m$ and $n = 1$ can be used to ensure the convergence of the diagnostic results. Because all required data are available from the CM1 output for all simulations, the dynamical efficiency is calculated using its original form Eq. (7) with the results shown in Fig. 6 for a reference. Note that the results discussed below are similar to those calculated with the simplified form of the dynamical efficiency Eq. (9). In addition, from the green dotted line in Fig. 2, $n = 1$ gives a linear relationship between IP and storm intensity in terms of maximum 10-m wind speed, consistent with the nearly linear relationship between the dynamical efficiency and the TC intensity from the numerical experiments (Fig. 6). This nearly linear relation is in fairly agreement with results from previous studies based on balanced dynamics (Schubert and Hack 1982, 1983; Pendergrass and Willoughby 2009). Note that the variation of the RMW with time has been included in the calculation of dynamical efficiency here (Fig. 6), which is different from that assumed in Fig. 2. This partly explains why the relationship between the dynamical efficiency and the TC intensity in Fig. 6 is not exactly linear as shown in Fig. 2.

Figures 7 and 8 compare the simulated IR (IR_{sim}) given by the time tendency of maximum 10-m wind speed from the ensemble mean of the full-physics axisymmetric model simulated V_{max}, and that estimated from the energetically based dynamical system IR model Eq. (17) from all experiments, with the dynamical efficiency given by Eq. (7) and all other variables from the ensemble mean simulations, except n and H, which are chosen as discussed above. For all experiments, the estimated IR using the modified energetically based dynamical system model can capture well the evolution of the simulated IR. In particular, the energetically based IR model delivers good approximations to both the maximum IR and the intensity-dependence of the IR in the simulations as in observations mentioned in section 3. The simplified dynamical system IR model gives a maximum IR between 30-50 m $s^{-1}d^{-1}$ around the intermediate intensity for each experiment, which agrees well with the model simulations and also fairly consistent with observations (Fig. 1). For both basins, both the estimated maximum IR and the intensity at the maximum IR (V_{mpir}) tend to increase with increasing SST, which is also in agreement with the model simulations (Figs. 7 and 8) and observations (Fig. 1).

To further ensure the robustness of the dynamical system model and the selections of n and H, several additional sensitivity ensemble experiments were performed. Those sensitivity experiments are the same as SST28_WNP, but with the latitude of f-plane decreased to 10°N (labeled as SST28_WNP_10N) and increased to 30°N (labeled as SST28_WNP_30N), with the RMW of the initial TC vortex decreased to 60 km (labeled as SST28_WNP_60km) and increased to 100 km (labeled as SST28_WNP_100km), with the enthalpy exchange coefficient halved (labeled as SST28_WNP_CK05) and doubled (labeled as SST28_WNP_CK20), with the horizontal mixing length halved (labeled as SST28_WNP_lh05) and doubled (labeled as SST28_WNP_lh20), and with the asymptotic vertical mixing length halved (labeled as SST28_WNP_lv05) and doubled (labeled as SST28_WNP_lv20). The simulated IR and estimated IR from Eq. (17) with $H = 2000\ m$ and $n = 1$ from those sensitivity experiments are shown in Fig. 9. As expected, for all experiments, the estimated IR can capture well the evolution of the simulated IR, and gives a maximum IR at the intermediate intensity as in the model simulations. Considering the simplicity of the energetically based dynamical system model, the discrepancies between the simulated IR and the estimated IR from Eq. (17) seem to be acceptable. The simplified energetically based IR model ignores any detailed dynamics that may cause short-term variability in intensity change. Even though the IR behavior related to small-scale motions is not considered, the IR equation proposed in this study is able to deliver a reasonable estimate for the upper IR limit, and the overall IR dependency on TC intensity as found in observations.

4. Conclusions and discussion

A pronounced feature from recent statistical analyses based on best-track TC data is that the maximum IR is observed most frequently when the maximum sustained surface wind speed of a TC is at an intermediate intensity of about 30-40 m s^{-1} (Kaplan et al. 2010; Xu and Wang 2015, 2018a). Such an intensity-dependence of the TC IR was previously explained qualitatively in terms of a core heating efficiency that enhances with the storm's intensity due to higher inner-core inertial stability on one hand, and less room for the storm to further intensify as it approaches its MPI on the other hand (Kaplan et al. 2010). Moreover, in several studies, time-dependent equations for the maximum near-surface wind speed (DeMaria 2009; Emanuel 1997, 2012; Ozawa and Shimokawa 2015; Emanuel and Zhang 2017) were derived. Although the logistical growth equation-based model of DeMaria (2009) and the modified theoretical model of Emanuel and Zhang (2017) from Emanuel (2012) could capture the overall evolution of TC intensity, the intensity-dependence of the TC IR was not discussed in these studies, which mainly focused on the environmental factors rather than the TC intrinsic dynamical parameters.

In this study, an empirical dynamical efficiency has been introduced to the simple energetically based model recently proposed by Ozawa and Shimokawa (2015). This simple model is based conceptually on the viewpoint that a TC can be described energetically as a Carnot heat engine in a non-steady state framework (Wang 2012, 2015). Here we have augmented this concept by introducing an empirical dynamical efficiency factor, which is presumed to be a function of the inner-core inertial stability, and to estimate the inner-core heating efficiency along with earlier theoretical studies based on balanced dynamics of TC intensification (Schubert and Hack 1982, 1983; Pendergrass and Willoughby 2009). With the introduced dynamical efficiency, the modified energetically based dynamical system model can explain and quantify the observed intensity-dependence of the TC IR fairly well.

According to the modified simple energetically based IR model, the TC IR is controlled by the intensification potential and the weakening rate due to surface friction beneath the eyewall. The intensification potential is determined primarily by the potential energy available for a TC to develop, which is a function of the thermodynamic conditions of the atmosphere and the underlying ocean, and the dynamical efficiency of the TC system. The latter factor, which we introduced in this study, depends strongly on the degree of convective organization within the eyewall and the inner-core inertial stability of the storm. At relatively weak intensity, the intensification potential of the intensifying storm is larger than the frictional weakening rate, leading to an increase in the TC IR with TC intensity in the initial stage. As the storm reaches an intermediate intensity of about 30–40 m s^{-1}, the difference between the intensification potential and frictional weakening rate reaches its maximum, concurrent with the maximum IR, or "maximum potential IR (MPIR)", of the TC. Later on, as the TC intensifies further, the IR decreases because surface friction increases with TC intensity at a faster rate than the intensification potential. Finally, as the storm approaches its MPI, the IR becomes zero.

The modified energetically based IR model is further validated with results from idealized ensemble full-physics model simulations with a nonhydrostatic, convection-resolving TC model. The full-physics model simulations reproduce the observed intensity-dependence of the TC IR reasonably well. Results from the estimated IR using the energetically based IR equation show that the net energy gain beneath the eyewall fits well the IR of the simulated storm. It is also shown that the modified simplified energetically based IR model reproduces the overall IR of the simulated storm. Although some discrepancies exist between the IR in the full-physics model simulations and that estimated from the simplified energetically based IR model due to its lack of any detailed dynamics, the simplified energetically based IR model may provide an estimate of the IR of a TC in its transient stage. It captures the major features of the intensity-dependence of the TC IR and its upper limit as evident from observations. Moreover, since the maximum potential IR is proportional to the MPI of the TC and the TC MPI is a function of SST and other environmental parameters, we may expect a trend in MPIR in response to environmental changes similar to that found for MPI (e.g., DeMaria and Kaplan 1994; Emanuel 1988). Hence, with view to many studies that have indicated possible increase in the MPI in the projected future climate, the modified simple energetically based dynamical system model of TC IR implies a correspondingly potential increase in TC IR in response to global warming as discussed by Emanuel (2017).

Finally, we should mention that in this study we have not considered any detrimental effects from unfavorable environmental conditions on TC IR. Therefore, the dynamical efficiency introduced in this study is purely an ad-hoc parameterization related to the inner-core dynamics of the TC itself. In this sense, we can consider the inner-core inertial stability determined dynamical efficiency as the intrinsic dynamical efficiency. This intrinsic dynamical efficient is the maximum efficiency of real TCs and thus the simplified energetically based IR model can provide the maximum possible IR at all stages of an intensifying TC. In our future studies, we will further introduce factors that may reduce the dynamical efficiency of the TC system, such as environmental vertical wind shear, the TC-induced ocean cooling, the convective activity outside the inner core, and so on. In addition, additional effort is under way to estimate parameters/constants in the simplified energetically based IR model using the best track TC data and statistical analysis, including machine learning algorithm. The results will be reported separately in due course.

Acknowledgments: The authors are grateful to two anonymous reviewers for their constructive comments. This study was supported in part by NSF grant AGS-1834300 and in part by National Natural Science Foundation of China under grants 41730960 and the National Key R&D Program of China under grant 2017YFC1501602. Y. Li was funded by China Scholarship Council (File 201806210324).

References

Bister, M., and K. A. Emanuel, 1998: Dissipative heating and hurricane intensity. *Meteor. Atmos. Phys*., **80**, 131–164, doi:10.1007/BF01030791.

Bryan, G. H., and J. M. Fritsch, 2002: A benchmark simulation for moist nonhydrostatic numerical model. *Mon. Wea. Rev.*, **130**, 2917–2928, doi:10.1175/1520-0493(2002)130<2917:ABSFMN>2.0.CO;2.

Carrasco, C., C. Landsea, and Y. Lin, 2014: The influence of tropical cyclone size on its intensification. *Wea. Forecasting*, **29,** 582–590, doi:10.1175/WAF-D-13-00092.1.

Charney, J. G., and A. Eliassen, 1964: On the growth of the hurricane depression. *J. Atmos. Sci.*, **21**, 68–75.

DeMaria, M. 2009: A simplified dynamical system for tropical cyclone intensity prediction. *Mon. Wea. Rev.*, **137**, 68–82, doi:10.1175/2008MWR2513.1

DeMaria, M., and J. Kaplan, 1994: Sea surface temperature and the maximum intensity of Atlantic tropical cyclones. *J. Climate,* **7,** 1325–1334, doi:10.1175/1520-0442(1994)007<1324:SSTATM>2.0.CO;2.

Donelan, M. A., B. K. Haus, N. Reul, W. J. Plant, M. Stiassnie, H. C. Graber, O. B. Brown, and E. S. Saltzman, 2004: On the limiting aerodynamic roughness of the ocean in very strong winds. *Geophys. Res. Lett.*, **31**, L18306, doi:10.1029/ 2004GL019460.

Emanuel, K. A., 1988: The maximum intensity of hurricanes. *J. Atmos. Sci*., **45**, 1143–1155, doi: 10.1175/1520-0469(1988)045<1143:TMIOH>2.0.CO;2.

Emanuel, K. A., 1989: The finite-amplitude nature of tropical cyclogenesis. *J. Atmos. Sci.*, **46**, 3431–3456, doi:10.1175/1520-0469(1989)046<3431:TFANOT>2.0.CO;2.

Emanuel, K. A., 1995: The behavior of a simple hurricane model using a convective scheme based on subcloud-layer entropy equilibrium. *J. Atmos. Sci.*, **52**, 3960–3968, doi: 10.1175/1520-0469(1995)052<3960:TBOASH>2.0.CO;2.

Emanuel, K. A., 1997: Some aspects of hurricane inner-core dynamics and energetics. *J. Atmos. Sci.*, **54**, 1014–1026, doi:10.1175/1520-0469(1997)054<1014:SAOHIC>2.0.CO;2.

Emanuel, K. A., 2012: Self-stratification of tropical cyclone outflow: Part II: Implications to storm intensification. *J. Atmos. Sci.*, **69**, 988–996, doi:10.1175/JAS-D-11-0177.1.

Emanuel, K. A., 2017: Will global warming make hurricane forecasting more difficult? *Bull. Amer. Meteor. Soc.*, **98**, 495–501, doi:10.1175/BAMS-D-16-0134.1.

Emanuel, K. A., J. D. Neelin, and C. S. Bretherton, 1994: On large-scale circulations in convecting atmosphere. *Q. J. Roy. Meteor. Soc*., **120**, 1111–1144, doi: 10.1002/qj.49712051902.

Emanuel, K. and F. Zhang, 2017: The Role of Inner-core moisture in tropical cyclone predictability and practical forecast skill. *J. Atmos. Sci.,* **74**, 2315–2324, doi:10.1175/JAS-D-17-0008.1.

Gray, W., M., 1979: Hurricanes: their formation, structure and likely role in the tropical circulation. *Meteorology over the Tropical Oceans,* D. B. Shaw, Ed., Royal Meteorological Society, James Glaisher House, Grenville Place, Bracknell, Berkshire, 155 – 218.

Kaplan, J., M. DeMaria, and J. A. Knaff, 2010: A revised tropical cyclone rapid intensification index for the Atlantic and eastern North Pacific basins. *Wea. Forecasting*, **25**, 220–241, doi: 10.1175/2009WAF2222280.1.

Kleinschmidt, E., 1951: Grundlagen eine Theorie der tropischen Zyklonen. *Meteor. Atmos. Phys.*, **4**, 53–72.

Li, Y., Y. Wang, and Y. Lin, 2019: Revisiting the dynamics of eyewall contraction of tropical cyclones. *J. Atmos. Sci.*, **76**, 3229–3245, doi:10.1175/JAS-D-19-0076.1.

Li, Y., Y. Wang, Y. Lin, R. Fei, 2020: Dependence of superintensity of tropical cyclone on SST in axisymmetric numerical simulations. *Mon. Wea. Rev.*, **148**, 4767–4781, doi: 10.1175/MWR-D-20-0141.1.

Montgomery, M. T., S. V. Nguyen, R. K. Smith, and J. Persing, 2009: Do tropical cyclone intensify by WISHE?, *Q. J. Roy. Meteorol. Soc*., **135**, 1697–1714, doi:10.1002/qj.459.

Montgomery, M. T., and R. K. Smith, 2014: Paradigms for tropical cyclone intensification. *Aust. Meteor. Ocean.*, *(Bruce Morton Memorial Volume)*, **64**, 37–66.

Nguyen, S. V., R. K. Smith, and M. T. Montgomery, 2008: Tropical cyclone intensification and predictability in three dimensions. *Q. J. Roy. Meteor. Soc.*, **134**, 563–582, doi:10.1002/qj.235.

Ooyama, K., 1964: A dynamical model for the study of tropical cyclone development. *Geofis. Int.*, **4**, 187–198.

Ooyama, K., 1969: Numerical simulation of the life cycle of tropical cyclones. *J. Atmos. Sci.*, **26**, 3–40, doi:10.1175/1520-0469(1969)026<0003:NSOTLC>2.0.CO;2.

Ooyama, K., 1982: Conceptual evolution of the theory and modeling of the tropical cyclone. *J. Meteor. Soc. Japan*, **60**, 369–379.

Ozawa, H., and S. Shimokawa, 2015: Thermodynamics of a tropical cyclone: generation and dissipation of mechanical energy in a self-driven convection system. *Tellus A*, **67**, 24216, doi: 10.3402/tellusa.v67.24216.

Pendergrass, A. G., and H. E. Willoughby, 2009: Diabatically induced secondary flows in tropical cyclones. Part I: Quasi-steady forcing. *Mon. Wea. Rev.*, **137**, 805–821, doi: 10.1175/2008MWR2657.1.

Rogers R., P. Reasor, and S. Lorsolo, 2013: Airborne doppler observations of the inner-core structural differences between intensifying and steady-state tropical cyclones. *Mon. Wea. Rev.,* **141**, 2970–2991, doi:10.1175/MWR-D-12-00357.1.

Rotunno, R., and K. A. Emanuel, 1987: An air-sea interaction theory for tropical cyclones. Part II: Evolutionary study using a nonhydrostatic axisymmetric model. *J. Atmos. Sci*., **44**, 542–561, doi:10.1175/1520-0469(1987)044<0542:AAITFT>2.0.CO;2.

Schönemann D. and T. Frisius, 2012: Dynamical system analysis of a low-order tropical cyclone model. *Tellus A*, **64**, 15817, doi:10.3402/tellusa.v64i0.15817.

Schubert W. H., and J. J. Hack, 1982: Inertial stability and tropical cyclone development. *J. Atmos. Sci.,* **39**, 1687-1697, doi: 10.1175/1520-0469(1982)039<1687:ISATCD>2.0.CO;2.

Schubert W. H., and J. J. Hack, 1983: Transformed Eliassen balanced vortex model. *J. Atmos. Sci.,* **40**, 1571-1583, doi:1520-0469(1983)040%3C1571:TEBVM%3E2.0.CO;2.

Shapiro L. J., and H. E. Willoughby, 1982: The response of balanced hurricanes to local sources of heat and momentum. *J. Atmos. Sci.,* **39**, 378–394, doi:10.1175/1520-0469(1982)039<0378:TROBHT>2.0.CO;2.

Smith, R. K., M. T. Montgomery, and V. S. Nguyen, 2009: Tropical cyclone spin up revisited. *Q. J. Roy. Meteor. Soc*., **135**, 1321–1335, doi:10.1002/qj.428.

Stern, D. P., J. L. Vigh, D. S. Nolan, and F. Zhang, 2015: Revisiting the relationship between eyewall contraction and intensification. *J. Atmos. Sci*., **72**, 1283–1306, doi:10.1175/JAS-D-

14-0261.1.

Thompson, G., P. R. Field, R. M. Rasmussen, and W. D. Hall, 2008: Explicit forecasts of winter precipitation using an improved bulk microphysics scheme. Part II: Implementation of a new snow parameterization. *Mon. Wea. Rev.*, **136**, 5095–5115, https://doi.org/10.1175/2008MWR2387.1.

Vigh J. L., and W. H. Schubert, 2009: Rapid development of the tropical cyclone warm core. *J. Atmos. Sc.*, **66**, 3335–3350, doi:10.1175/2009JAS3092.1.

Wang, Y., 2012: Recent research progress on tropical cyclone structure and intensity. *Tropical cyclone Res. Rev*., **1**, 254–275. doi:10.6057/2012TCRR02.05.

Wang, Y., 2015: Hurricane Dynamics. *Encyclopedia of Atmospheric Sciences*, 2nd edition, Vol. 6, 8–29, Gerald R. North (editor-in-chief), John Pyle and Fuqing Zhang (editors). Elsevier Ltd, doi:10.1016/B978-0-12-382225-3.00488-6.

Wang, Y., and C.-C. Wu, 2004: Current understanding of tropical cyclone structure and intensity changes – A review. *Meteor. Atmos. Phys*., **87**, 257–278, doi: 10.1007/s00703-003-0055-6.

Wang, Y., and J. Xu., 2010: Energy production, frictional dissipation, and maximum intensity of a numerically simulated tropical cyclone. *J. Atmos. Sci.*, **67**, 97–116, doi: 10.1175/2009JAS3143.1.

Xu, J., and Y. Wang, 2015: A statistical analysis on the dependence of tropical cyclone intensification rate on the storm intensity and size in the North Atlantic. *Wea. Forecasting*, **30**, 692–701, doi:10.1175/WAF-D-14-00141.1.

Xu, J., and Y. Wang, 2018a: Dependence of tropical cyclone intensification rate on sea surface temperature, storm intensity, and size in the western North Pacific. *Wea. Forecasting*, **33**, 523–537, doi:10.1175/WAF-D-17-0095.1

Xu, J., and Y. Wang, 2018b: Effects of the initial vortex structure on intensification of a numerically simulated tropical cyclone. *J. Meteor. Soc. Japan*, 96, 111–126, doi: 10.2151/jmsj.2018-014.

Zhang, J. A., R. F. Rogers, D. S. Nolan, F. D. Marks, 2011: On the characteristic height scales of the hurricane boundary layer. *Mon. Wea. Rev.*, **139**, 2523–2535, doi:10.1175/MWR-D-10-05017.1.

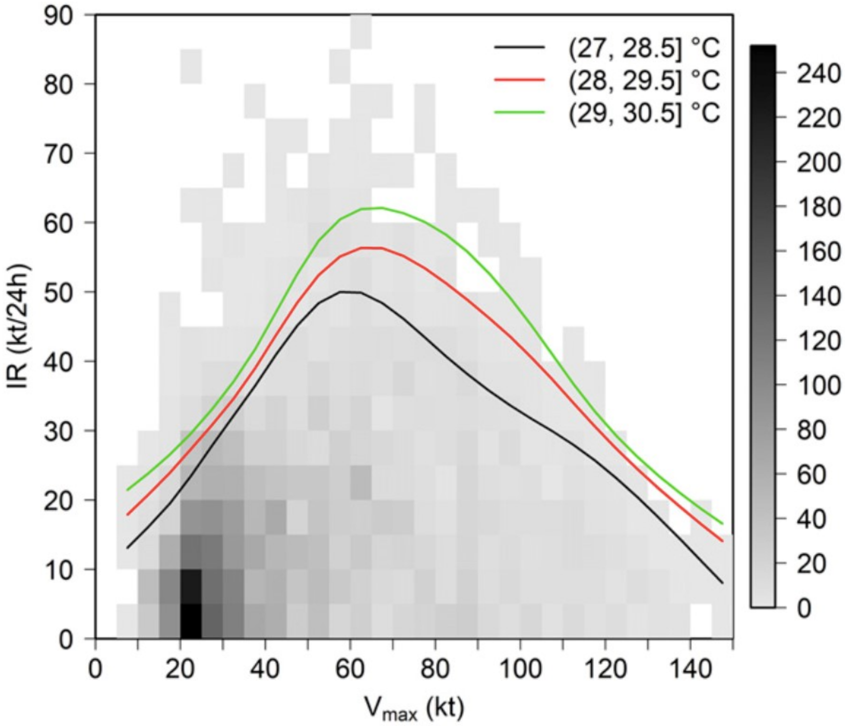

Figure 1: Frequency of the subsequent 24-h intensification rate (IR) against instantaneous storm intensity (V_{max} in terms of maximum 1-min mean sustained 10-m wind speed) with the black, red, and green curves showing the spline fitted curves for the 95th percentile of IR for three 1.5°C intervals of SST starting at 27, 28, and 29°C, respectively (reproduced from Fig. 6 of Xu and Wang 2018a).

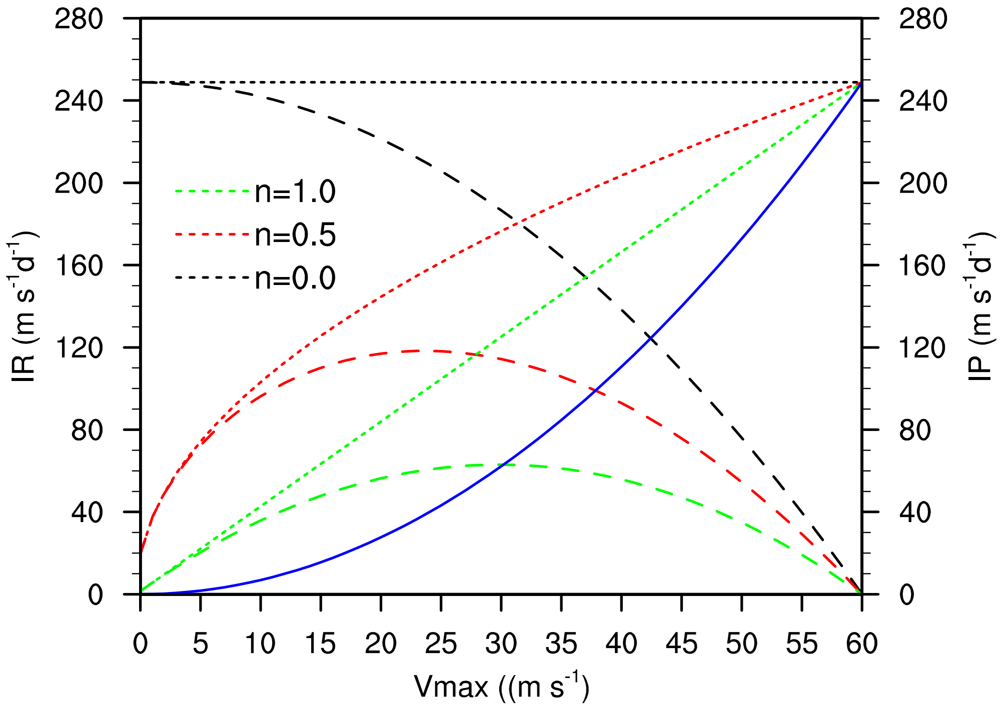

Figure 2. Dependence of the TC intensification rate (IR in m s^{-1} d^{-1}, dashed curves, left Y axis) on the TC intensity V_{max}, with V_{mpi} = 60 m s^{-1}, and r_{mpi} = 15 km for three cases, which differ in the dependence of intensification potential (IP) on dynamical efficiency E with n = 0.0 (black curves), n = 0.5 (red curves), and n = 1.0 (green curves). The corresponding IPs (m s^{-1} d^{-1}, dotted curves, right Y axis) and the frictional weakening rate (FR in m s^{-1} d^{-1}, solid blue curve, right Y axis) are also shown. The V_{mpi} of 60 m s^{-1} is obtained for T_S=29°C, C_D=2.4×10^{-3}, C_k=1.2×10^{-3}, and a sounding with the convective available potential energy of about 1900 J. For simplification, the RMW (r_m) of the intensifying storm in the dynamical efficiency calculation [cf. Eq. (9)] is assumed to be constant and equal to r_{mpi}. See text for further references.

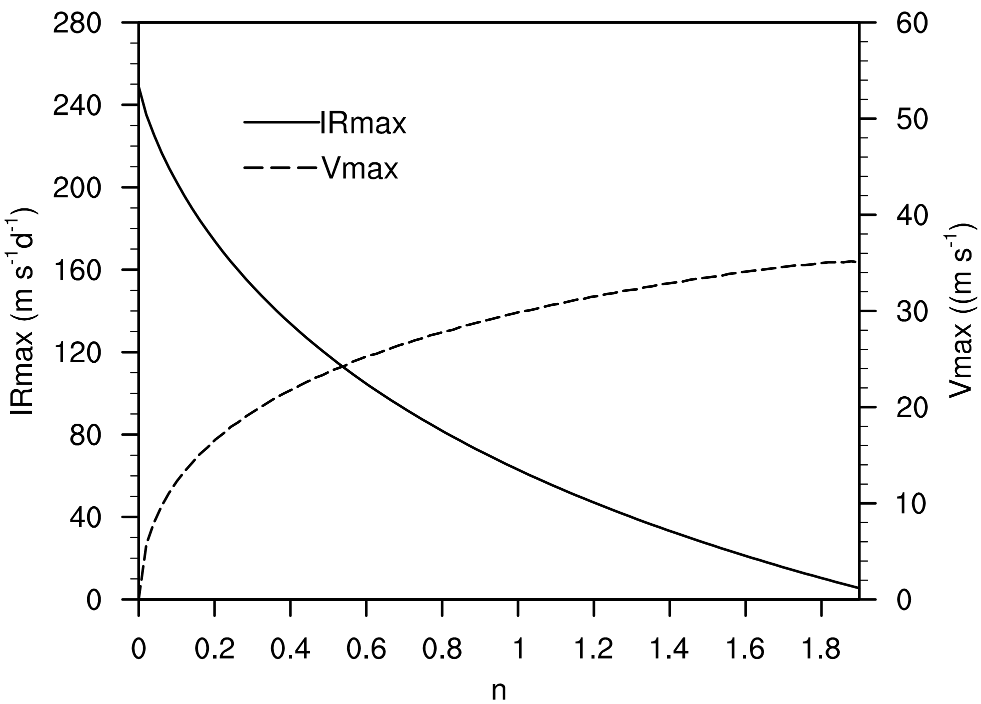

Figure 3. Maximum intensification rate (IR$_{max}$ in m s^{-1}d^{-1}, solid curve, left Y axis) and corresponding storm intensity (V_{max} in m s^{-1}, dashed curve, right Y axis) as a function of power index n, which sets the dependency degree of the IP on dynamical efficiency E defined by the normalized inertial stability frequency. Other parameters are the same as those chosen in the calculations for Fig. 2.

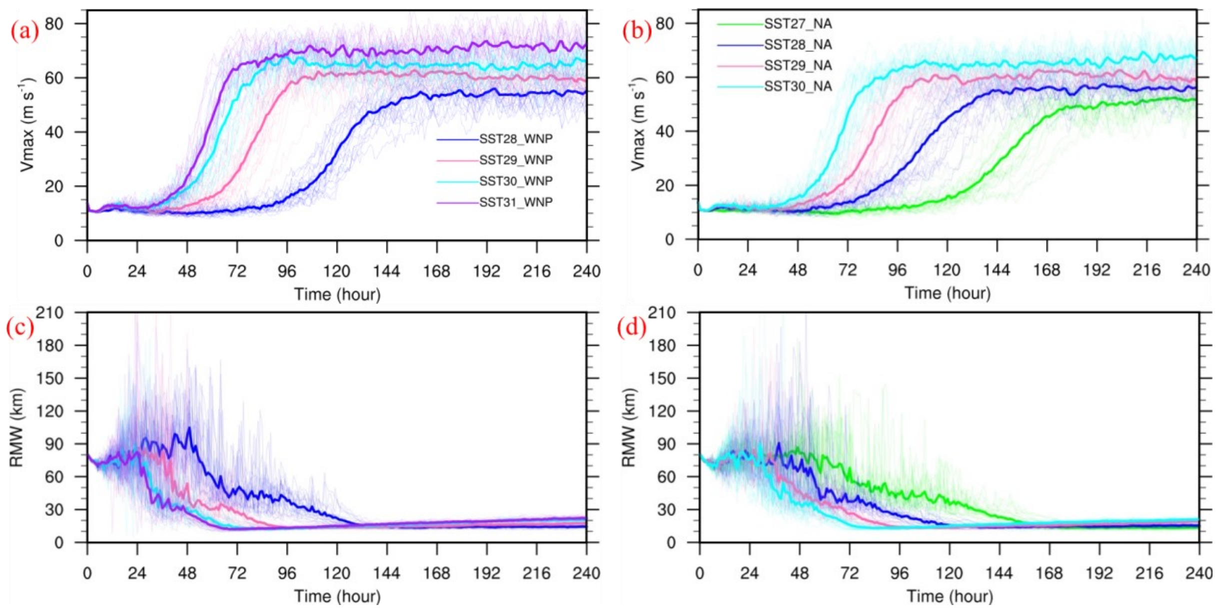

Figure 4. Time evolution of (a–b) maximum 10-m wind speeds and (c–d) corresponding radii of maximum wind in ensemble simulations (thin curves) and their corresponding ensemble averages (thick curves) for experiments using the SST-sorted atmospheric soundings (a, c) over the western North Pacific and (b, d) over the North Atlantic, respectively.

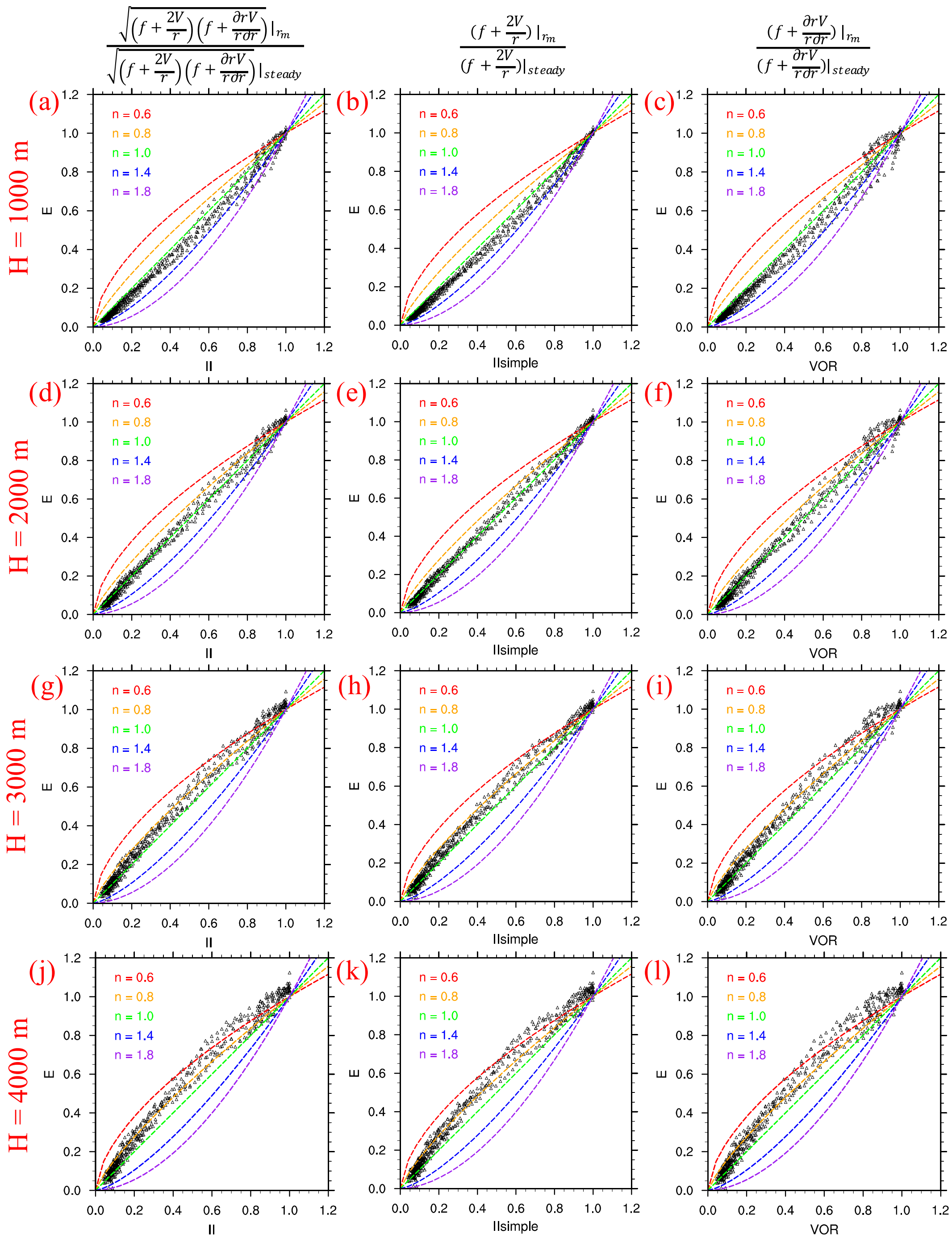

Figure 5. Scatter diagram of the diagnosed dynamical efficiency based on Eq. (17) against (a,d,g,j) normalized inertial stability in Eq. (7), (b,e,h,k) normalized simplified inertial stability in Eq. (9), and (c,f,i,l) normalized absolute vorticity for (a–c) $H = 1000$ m, (d–f) $H = 2000$ m, (g–i) $H = 3000$ m, and (j–l) $H = 4000$ m.

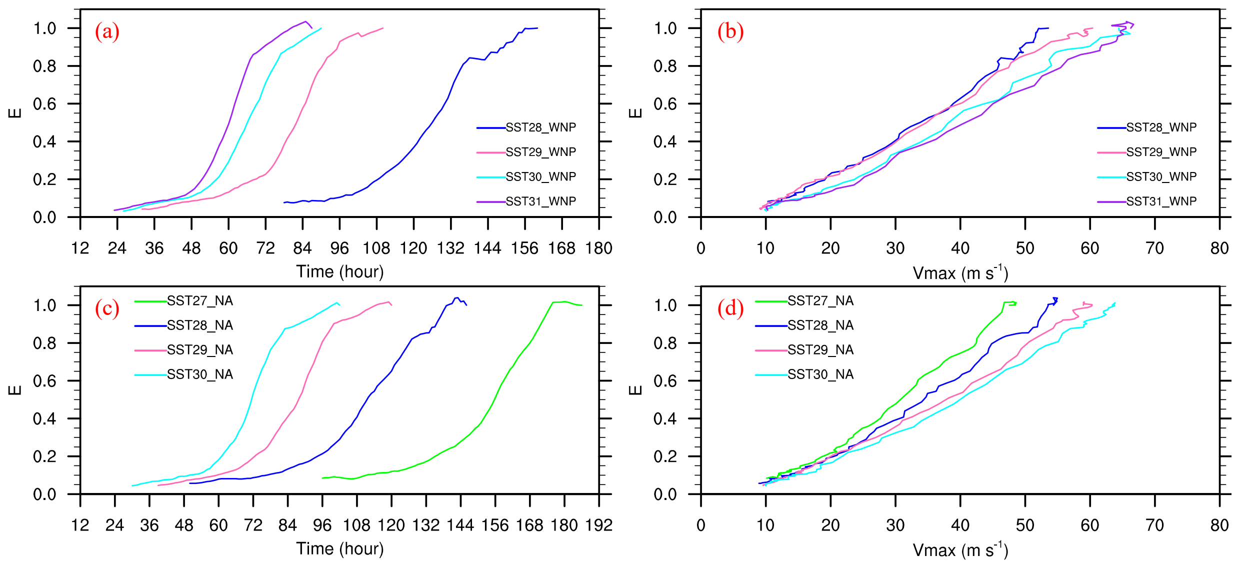

Figure 6. The dynamical efficiency E estimated using Eq. (7) as a function of (a, c) time and (b, d) the simulated ensemble mean maximum 10-m wind speed based on the ensemble mean results for experiments using the SST-sorted atmospheric soundings (a, b) over the western North Pacific and (c, d) over the North Atlantic, respectively.

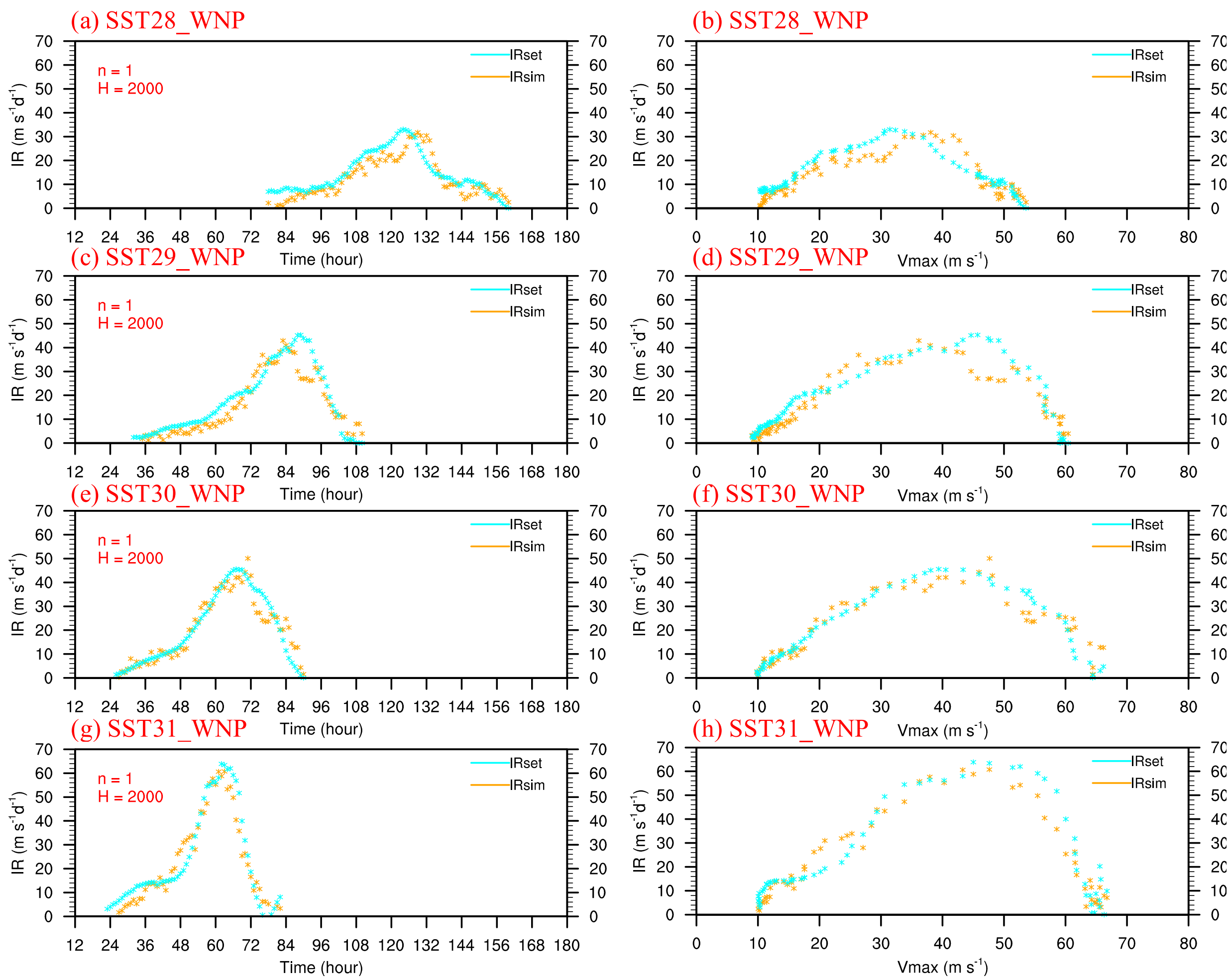

Figure 7. (a,c,e,g) Time evolution of the simulated ensemble mean maximum 10-m wind speed tendency (IR_{sim} in m s^{-1} d^{-1}, orange curve) and the estimated intensification rate according to the energetic intensification rate by Eq. (17) (IR_{est} in m s^{-1} d^{-1}, cyan curve) from experiments using the SST-sorted atmospheric soundings over the western North Pacific, and (b,d,f,h) IR_{sim} (m s^{-1} d^{-1}, orange curve) and IR_{est} (m s^{-1} d^{-1}, cyan curve) as a function of the simulated ensemble mean maximum 10-m wind speed (x-axis: V_{max} in m s^{-1}). Besides H and n, all variables used to calculate the estimated IR are taken from the ensemble mean simulations. The dynamical efficiency E is estimated using Eq. (7). See text for further details.

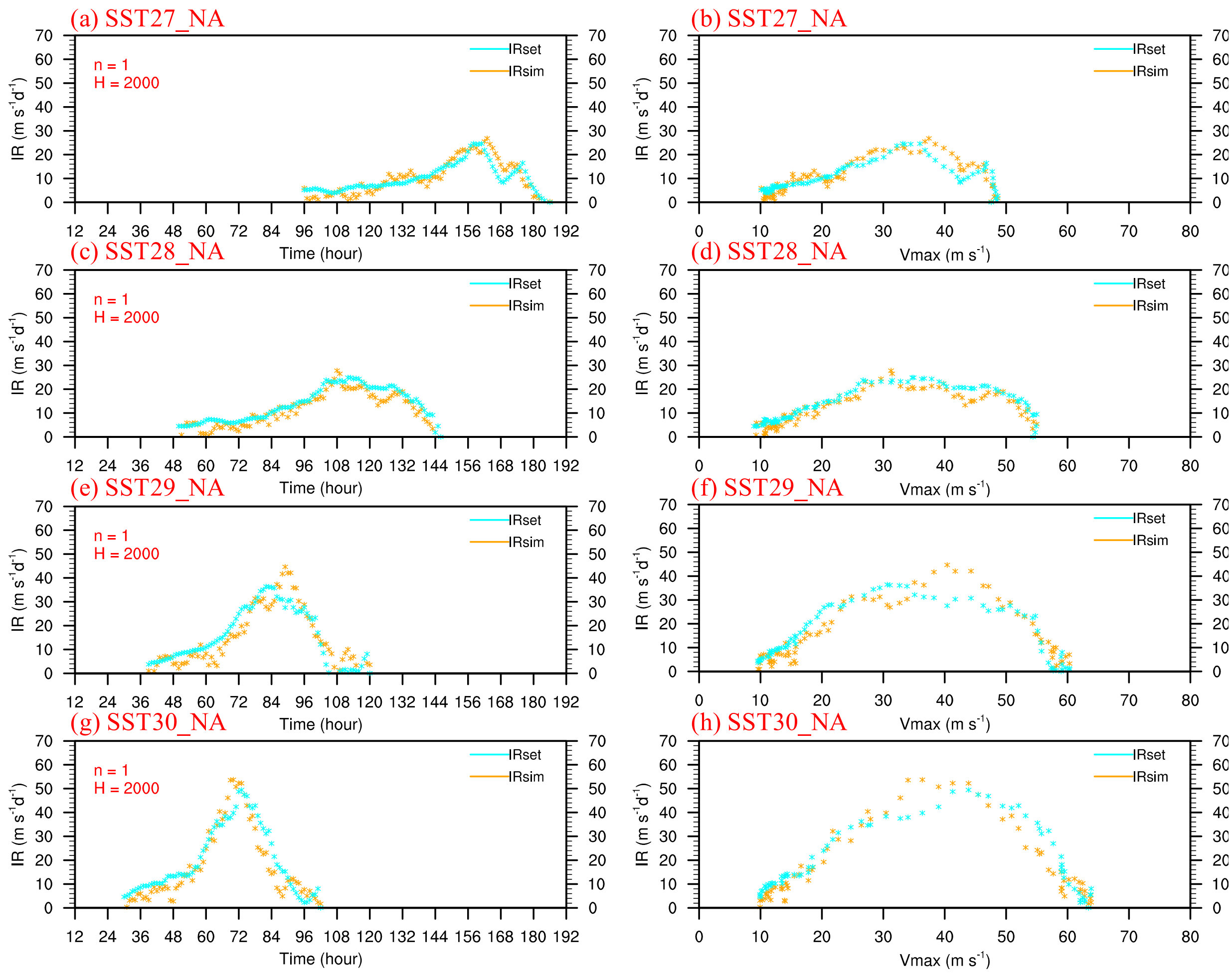

Figure 8. As in Fig. 7 but for experiments using the SST-sorted atmospheric soundings over the North Atlantic.

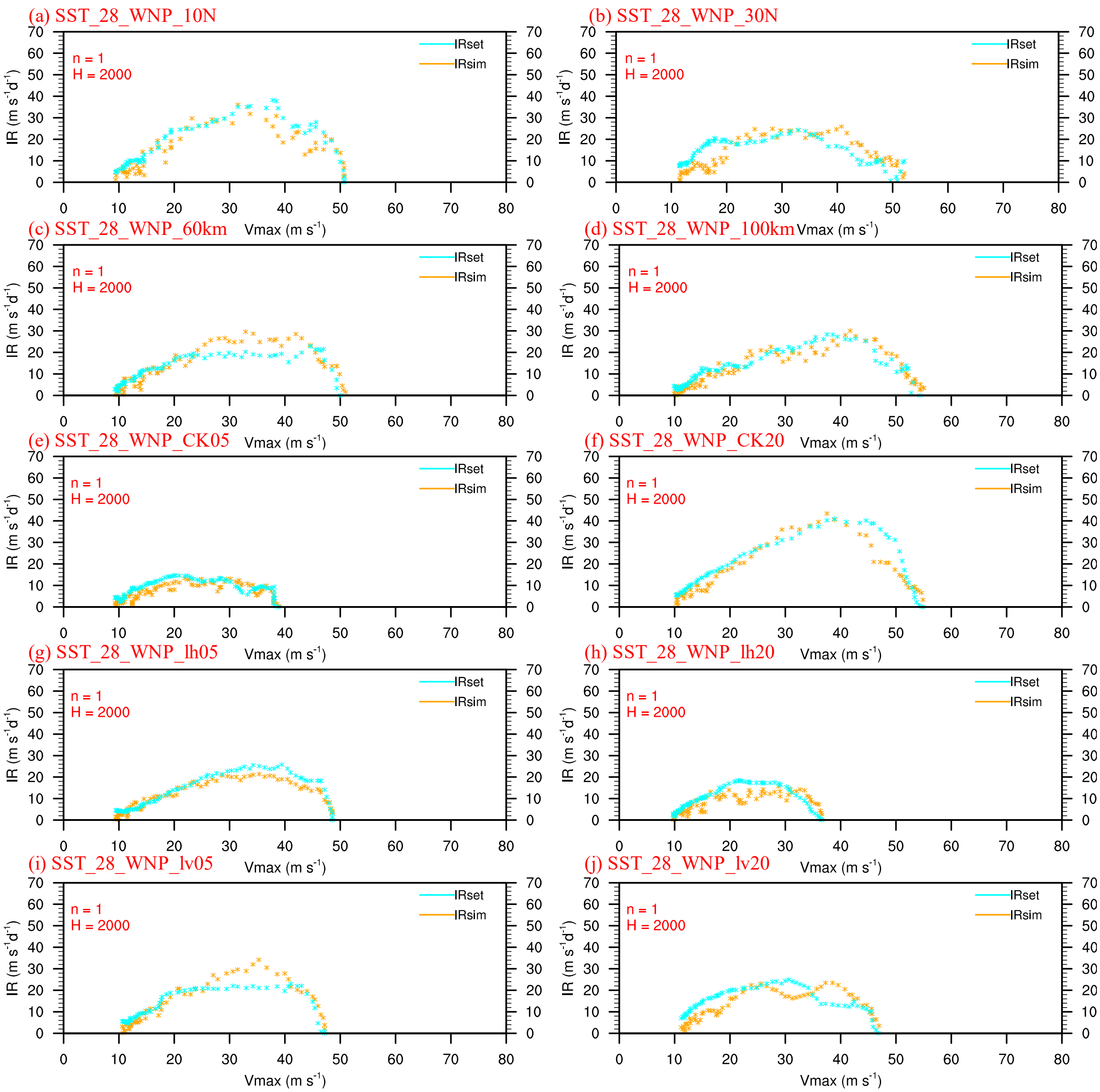

660

661 Figure 9. As in Fig. 7b, but from different sensitivity experiments as indicated by the legends.